Chemical Science

EDGE ARTICLE

View Article Online
View Journal | View Issue

Cite this: *Chem. Sci.*, 2018, **9**, 8446

All publication charges for this article have been paid for by the Royal Society of Chemistry

Thermo- and photo-modulation of exciplex fluorescence in a 3D spin crossover Hofmann-type coordination polymer†

Teresa Delgado,‡[a] Manuel Meneses-Sánchez,‡[b] Lucía Piñeiro-López,[b] Carlos Bartual-Murgui,[b] M. Carmen Muñoz[c] and José Antonio Real *[b]

The search for bifunctional materials showing synergies between spin crossover (SCO) and luminescence has attracted substantial interest since they could be promising platforms for new switching electronic and optical technologies. In this context, we present the first three-dimensional Fe^{II} Hofmann-type coordination polymer exhibiting SCO properties and luminescence. The complex $\{Fe^{II}(bpben)[Au(CN)_2]\}$@pyr (bpben = 1,4-bis(4-pyridyl)benzene) functionalized with pyrene (pyr) guests undergoes a cooperative multi-step SCO, which has been investigated by single crystal X-ray diffraction, single crystal UV-Vis absorption spectroscopy, and magnetic and calorimetric measurements. The resulting fluorescence from pyrene and exciplex emissions are controlled by the thermal and light irradiation (LIESST effect) dependence of the high/low-spin state population of Fe^{II}. Conversely, the SCO can be tracked by monitoring the fluorescence emission. This ON–OFF interplay between SCO and luminescence combined with the amenability of Hofmann-type materials to be processed at the nano-scale may be relevant for the generation of SCO-based sensors, actuators and spintronic devices.

Received 18th June 2018
Accepted 7th September 2018

DOI: 10.1039/c8sc02677g

rsc.li/chemical-science

Introduction

Iron(II) spin crossover (SCO) complexes are responsive materials that switch between high-spin (HS) and low-spin (LS) states triggered by external stimuli (temperature, pressure, light, and analytes). This binary HS ↔ LS behaviour entails strong electron–phonon coupling that involves drastic changes in the magnetic, electric, optical and mechanical properties of the SCO material when cooperative elastic interactions between the SCO centres are effective.[1] Cooperative SCO properties have attracted substantial interest specially when combined in a synergistic way with other relevant physical properties (*i.e.* electronic transport, chirality, luminescence, host–guest chemistry, *etc*) because the intrinsic ON–OFF nature of SCO may be transferred to the second property. This fact, together with the amenability of the resulting functional material to be processed at micro- and nano-scale levels, has created important expectations for the discovery of new switching electronic and optical technologies.[2]

Luminescence is a relevant property that may be used as an internal probe to report upon the spin state of SCO centres and conversely the control of the spin state may be used to modulate the luminescent signal. In this respect, it has been stated that the search for synergies between SCO and luminescence could be an important platform for thermometry and thermal imaging technologies.[3] Although, the interplay between SCO and luminescence was first reported 20 years ago,[4] it has been more recently that this binomial has gained much attention. Two main approaches have been designed to combine SCO and fluorescence in the same material. A first approach introduces fluorescence as an extrinsic property by physically doping the targeted SCO complex with a fluorescent dye during the fabrication of thin films or nanoparticles.[5–10] In the second approach, luminescence is an intrinsic property of the SCO complex. Only a reduced number of examples of this second approach have been reported so far, which include discrete mononuclear[11–14] homodinuclear,[15] heterodinuclear Fe^{II}–Eu^{III},[4] heterotrinuclear Fe^{II}–Pt^{II},[16] and two 1-D coordination polymers.[17,18]

Hofmann-type Fe^{II} SCO coordination polymers (SCO-CP)[19,20] have afforded excellent examples of thermo-[21] and piezo-hysteretic behaviours,[22] multistep cooperative transitions,[23] relevant examples of porous systems where the SCO can be tuned by guest molecules favouring selective host–guest interactions,[24] post-synthetic chemical activity[25] and/or solid-state

[a]*Département de Chimie Physique, Université de Genève, Rue Ernest Ansermet, 30, 1211 Genève, Switzerland*

[b]*Departament de Química Inorgánica, Institut de Ciència Molecular (ICMol), Universitat de València, Catedrático José Beltrán Martínez, 2, 46980 Paterna, Spain*

[c]*Departamento de Física Aplicada, Universitat Politècnica de València, Camino de Vera s/n, 46022 Valencia, Spain*

† Electronic supplementary information (ESI) available: Experimental information, and synthesis and characterisation of materials (PDF). CCDC 1847351–1847353 & 1862017. For ESI and crystallographic data in CIF or other electronic format see DOI: 10.1039/c8sc02677g

‡ These authors contributed equally.

transformations.[26] In addition, they have demonstrated to be excellent platforms to investigate the SCO properties at the nano-scale (nanocrystals and thin films) as potential components for the generation of SCO-based sensors, actuators and spintronic devices.[27] In this context, and as a result of our systematic study on Hofmann-type Fe^{II} SCO-CP,[19] here we report on the thermo- and photo-induced multi-stable spin transition of a pyrene based 3-D Hofmann clathrate monitored by photoluminescence and on the corresponding thermo- and photo-modulation of the exciplex fluorescence emission. This study has been carried out based on single crystal UV-Vis absorption spectroscopy measurements, X-ray single crystal analysis at relevant temperatures and magnetic, photo-magnetic and calorimetric measurements on microcrystalline samples of the SCO-MOF $\{Fe^{II}(bpben)[Au(CN)_2]\}$@pyr [**1Fe@pyr**] (bpben = 1,4-bis(4-pyridyl)benzene; pyr = pyrene). For comparative reasons the homologous isostructural Zn^{II} derivative **1Zn@pyr** was also synthesised and characterised and herein reported. As far as we know this is the first SCO-CP implemented with luminescence properties.

Results and discussion

Synthesis and structure

Pale-yellow (**1Fe@pyr**) or white (**1Zn@pyr**) crystalline samples were obtained by slow diffusion methods from stoichiometric amounts of $M^{II}(BF_4)_2\cdot 6H_2O$ (M^{II} = Fe, Zn), bpben and $K[Au(CN)_2]$ and an excess of pyrene dissolved in methanol (see the ESI†).

Single crystal structure analysis of **1Fe@pyr** and **1Zn@pyr** at 120 and 280 K showed the non-centrosymmetric monoclinic space group *Cc*. Crystal data and structural parameters are given in Tables S1–S3 in the ESI.†

There are two crystallographically distinct octahedral $[M^{II}N_6]$ sites constituted of 4 equatorial $[Au(CN)_2]^-$ groups and 2 axial bpben ligands (Fig. S1†). The almost linear $[Au(CN)_2]^-$ groups bridge 4 equivalent $[M^{II}N_6]$ sites forming parallel stacks of $\{M_4^{II}[Au(CN)_2]_4\}_n$ 2D grids pillared by the bpben ligands, thus generating an open framework with **pcu** topology (Fig. 1). The wide $\{M_4^{II}[Au(CN)_2]_4\}$ windows allow interpenetration of an identical framework made up of the other crystallographically independent $[M^{II}N_6]$ site (Fig. 1). This type of structure is common for $\{Fe^{II}(L)[Au(CN)_2]\}$ SCO compounds where L is a bis-monodentate pyridine-type ligand.[19,20]

The two frameworks are held together by strong Au···Au interactions [average 3.0535(5) Å for **1Fe@pyr** and 3.1086(9) Å for **1Zn@pyr** at 120 K]. The average Fe–N bond length equal to 1.960 Å at 120 K and 2.154 Å at 280 K are typical of the Fe^{II} ion in the LS and HS states, respectively. Thus, the average bond length variation associated with the spin-state change, 0.2 Å, is consistent with the occurrence of a complete LS ↔ HS conversion. This is in turn reflected in a change of the unit cell volume of 444.7 $Å^3$, which represents 6.7% of the HS unit cell volume or a volume change of 55.6 $Å^3$ per Fe^{II} upon SCO. This is a typical value observed for Hofmann clathrates.[19] It is worth noting that, in the same interval of temperatures, a unit cell volume variation of 1% (68.4 $Å^3$) is observed for **1Zn@pyr**, which essentially corresponds to thermal contraction/expansion of the crystal in the temperature interval 280–120 K where the average Zn^{II}–N bond length remains practically constant at *ca.* 2.145 Å.

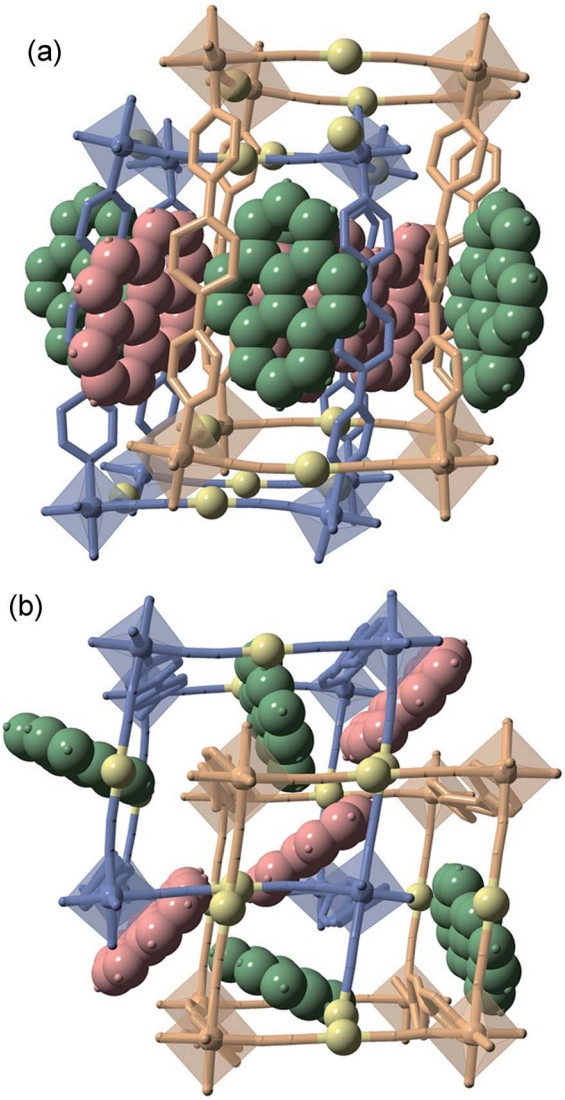

Fig. 1 Two perpendicular perspective views ((a) side view and (b) top view) of the same fragment of the doubly interpenetrated frameworks **1M@pyr** (M^{II} = Fe, Zn) showing the bpben pillars, coordination centres and pyrene units. The two crystallographically distinct frameworks are represented in blue (network 1) and beige (network 2) colours, while the different pyrene molecules are depicted in red (pyr1) and green (pyr2) colours. Au centres are yellow spheres.

The available space generated by the two interpenetrating frameworks is filled by two crystallographically independent pyr guest molecules that do not interact significantly with each other. In contrast, they define a large number of short π–π interactions with the bpben ligands (Fig. 2 and Table S4†). The number and strength of these interactions are unequally distributed in each framework. The bpben1 pillars attached to the $[Fe_1N_6]$ nodes (blue colour, Fig. 1 and 2) define with the corresponding pyr1 guests (red colour) a face-to-face type interaction with 22 short C···C contacts smaller than the sum of the van der Waals radius (*ca.* 3.7 Å) ranging in the interval

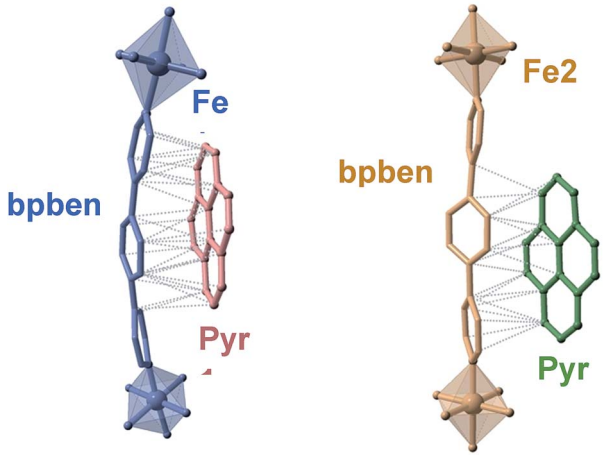

Fig. 2 Crystallographically different bpben-pyrene pairs found in **1Fe@pyr** displaying the intermolecular π–π interactions (dotted lines) between bpben and pyrene (only short π–π contacts smaller than the sum of the C···C van der Waals radius *ca.* 3.7 Å are shown).

[3.44–3.68 Å] at 280 K (Table S4, Fig. S2†). They markedly increase in number, up to 37 C···C contacts [3.30–3.66 Å], in the LS structure at 120 K (Fig. 2). It is worth noting that this increase in short π–π interactions occurs synchronically with a small in-plane rotation of the pyr1 by *ca.* 6.1° (Fig. S2†). In contrast, 22 [3.32–3.69 Å] and 12 [3.42–3.68 Å] short C···C contacts at 120 K and 280 K, respectively, are found between the bpben2 pillars attached to the $[Fe_2N_6]$ nodes (beige colour, Fig. 1 and 2) and the corresponding pyr2 (green colour). This *ca.* 50% decrease of C···C interactions is due to parallel-displaced π–π interactions in the latter. Although similar considerations can be made for **1Zn@pyr**, the larger ionic radius of Zn^{II} with respect to Fe^{II}-LS is reflected in a slight reduction in the number of π–π interactions (Table S4-bis, Fig. S2†).

A direct consequence of these strong π–π interactions is the bent geometry adopted by the bpben ligands. A similar situation was described for the SCO Hofmann clathrates $\{Fe(bpb)[M^{II}(CN)_4]\}\cdot 2G$, where the related rod-like bridging ligand bis(4-pyridyl)butadiyne (bpb) is markedly bent due to strong intermolecular interactions established with G = naphthalene or nitrobenzene molecules.[28] For the titular compounds, we have estimated the magnitude of the bent in bpben measuring the distance of the pyridyl N atoms to the average plane defined by the central benzene ring (see Table S5a and Scheme I†). It is important to note that the bent, and consequently the distance to the average plane, is larger for bpben1 than for bpben2 due to the larger number and more direct π–π interactions with pyr in the former. In addition to this, the pyridyl groups are slightly rotated with respect to the central benzene ring (Table S5b†). Both, the bent distortion and the angles defined by the intersection of the benzene and pyridyl rings do not change significantly upon the spin state change of Fe^{II}. Furthermore, these distances and angles are consistent with those found for **1Zn@pyr**. It is worth mentioning that the bent geometry found for the bpben pillars in the titular compounds strongly contrasts with the linear structure described previously for the solvate $[Fe(bpben)\{Au(CN)_2\}_2]\cdot S$ with $S = 1.5DMF\cdot 0.3EtOH\cdot 0.2C_6H_{12}$.[29]

Spin crossover behaviour

Magnetic, photo-magnetic and calorimetric studies. The SCO was followed by magnetic measurements on bulk samples in the temperature interval 10–300 K (Fig. 3). At room temperature, the $\chi_M T$ product (χ_M = molar magnetic susceptibility and T = temperature) equal to 3.64 $cm^3\ K\ mol^{-1}$ is consistent with the Fe^{II} ion in the HS state. On cooling at a temperature scan rate of 1 K min^{-1}, $\chi_M T$ drops abruptly between 250 and 160 K, in three consecutive steps centred at 227, 195 and 180 K, to 0.14 $cm^3\ K\ mol^{-1}$ indicating a practically complete transformation to the LS state. In the heating mode, the magnetic curve does not match the cooling curve showing the presence of hysteresis in the second and third steps *ca.* 5 K wide. The overall equilibrium temperature, $T_{1/2}$, at which the HS and LS molar fractions are equal to 0.5 ($\gamma_{HS} = \gamma_{LS} = 0.5$; $\Delta G = 0$) is estimated to be centred at 190 K. This multi-step SCO behaviour is reminiscent of the one previously observed for the homologue solvate $[Fe(bpben)\{Au(CN)_2\}_2]\cdot S$ with S = 0.9 benzene, which undergoes a less steep three-step conversion centred at 214 K, 155 K and 141 K.[29] The occurrence of multi-step SCO is a relatively uncommon event in SCO that results from a competition between ferro- and antiferro-elastic interactions driven by the difference of volume associated with the LS and HS centres.[30] The steps involve stabilization of states characterized by different commensurate and/or incommensurate ordered fractional distributions of the HS/LS sites that often require symmetry breaking and that dramatically depend on subtle structural changes of the solid, which are difficult to control.[31]

Irradiation of the sample with red light (λ = 633 nm) at 10 K photo-generates the metastable HS* state (light induced excited spin state trapping (LIESST),[32] see the green line in Fig. 3).

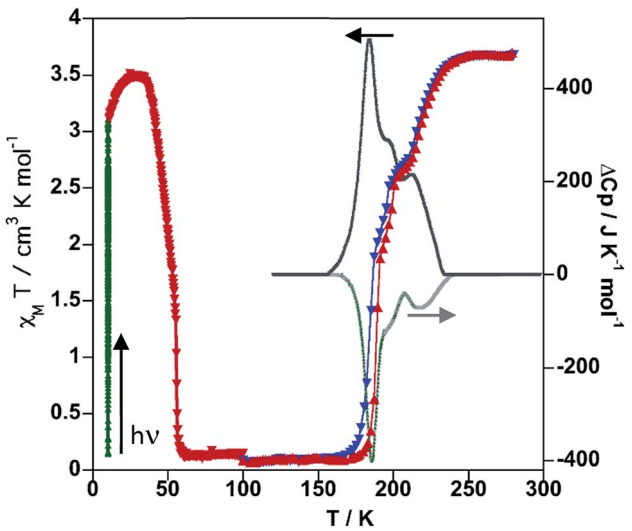

Fig. 3 Magnetic, photomagnetic and calorimetric properties of **1Fe@pyr**. Blue down triangles and red up triangles refer to cooling and heating modes, respectively. Green triangles show the increase of $\chi_M T$ upon irradiation at 10 K (LIESST effect), and red down triangles correspond to the heating from 10 K at 0.3 K min^{-1} to determine the T_{LIESST} temperature. Grey curves correspond to the anomalous variations of the molar specific heat C_p caused by the SCO for the cooling and heating modes.

The subsequent heating at 0.3 K min^{-1} in the dark shows an increase of $\chi_M T$, associated with the zero-field splitting of the S = 2 HS state of Fe^{II}, reaching a maximum value of 3.50 cm^3 K mol^{-1} in the temperature range 24–34 K, which suggests a quantitative population of the HS* state. Upon further heating the HS* relaxes back in two steps to the LS state with a characteristic $T_{LIESST} \approx 50$ K.[33]

The thermodynamic parameters obtained from differential scanning calorimetry were consistent with the $\chi_M T$ *vs.* T plot (grey lines in Fig. 3). The average enthalpy and entropy variations $\Delta H = 10.9$ kJ mol^{-1} and $\Delta S = 56$ J K^{-1} mol^{-1} are typical of Fe^{II} SCO compounds.

Single crystal UV-Vis spectra. 1Fe@pyr displays a reversible thermo-chromic change between pale-yellow (HS) and red (LS). Consequently, the SCO behaviour was monitored on a single crystal through UV-Vis absorption spectra in the temperature range 300–10 K (cooling and heating modes) with temperature scan rates of 1 and 5 K min^{-1} while recording the spectra every 1 and 5 min (see Fig. 4a, S3 and S4,† respectively). When cooling from 300 K to 10 K, the band centred at 800 nm associated with the HS state bleaches while a new band attributed to the LS state arises centred at 532 nm when cooling to 10 K. Considering the thickness of the crystal, 50 ± 1 μm, and a concentration of Fe of around 1.6 M, a typical value of ferrous spin crossover systems, an extinction coefficient, ε, equal to 7 and 125 M^{-1} cm^{-1} was found, respectively, for the 800 and 532 nm bands. These values are consistent with the d–d transitions $^5T_2 \rightarrow {}^5E$ and $^1A_1 \rightarrow {}^1T_1$ characteristic of the HS and LS states of Fe^{II}, respectively.

Following the optical density difference between the maximum of the LS band at 532 nm and the tail of this band at 650 nm, the evolution of the HS molar fraction (γ_{HS}) with temperature was stablished by using Vergard's law (eqn (1)).

$$\gamma_{HS} = (OD_{LS} - OD_T)/(OD_{LS} - OD_{HS}), \quad (1)$$

where OD_{LS} is the optical density of the LS state, OD_{HS} is the optical density of the HS state at 300 K and OD_T is the optical density at a given temperature. The optical density (OD) is corrected from an eventual baseline jump or shift by taking the difference between the OD at 532 nm and the OD at 650 nm, where there is no noticeable absorption in the two states. The resulting SCO profile displays three main steps centred at 230, 195 and 184 K (Fig. 4b). Irradiation of the crystal with green light (λ = 532 nm) at 10 K quantitatively photo-generates the metastable HS* state. The thermal stability of HS* was examined following the spectra when heating the crystal in the dark at 0.3 K min^{-1} from 10 to 60 K (Fig. 4b and S5†). The thermal relaxation HS* → LS was characterized by a $T_{LIESST} = 45$ K. Both, thermal- and photo-induced SCO behaviours agree reasonably well with the complementary magnetic measurements.

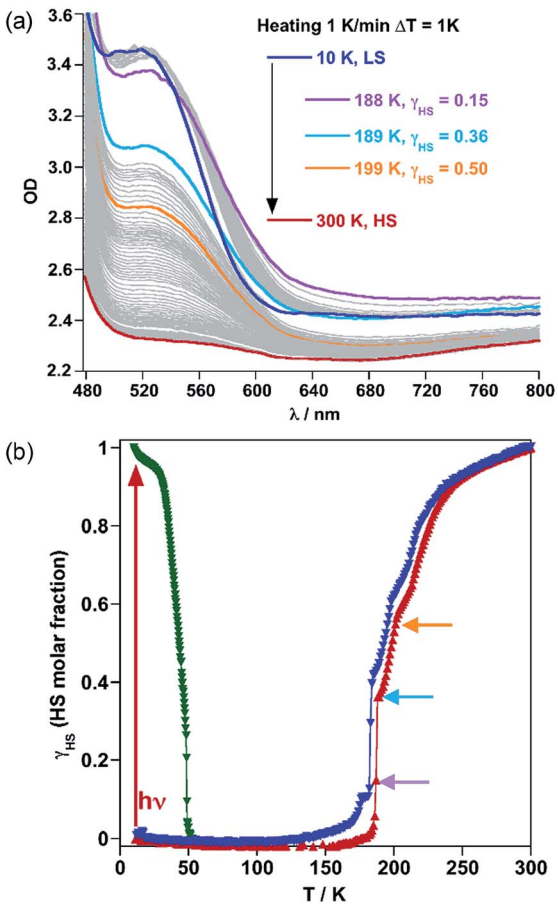

Fig. 4 SCO properties of **1Fe@pyr** monitored by using single crystal UV-Vis spectra: (a) temperature variable UV-Vis absorption spectrum in the cooling mode and (b) HS molar fraction of the thermal and light induced SCO.

Synergy between fluorescence and spin crossover

The crystal structure of **1Fe@pyr** reveals that the pyr guest molecules and bpben bridging ligands lie in an environment that is fully consistent to afford exciplex emission through π–π interactions.[34] Consistently with this, the excitation spectrum recorded at room temperature at 520 nm, shows a set of four different main bands, two of them highly resolved and centred at 254 and 332 nm. The other two bands are rather broad and centred at around 350 and 400 nm. Likewise, the emission spectrum of the sample has been recorded between 350 and 700 nm after excitation at 332 nm (Fig. S6†). The two characteristic bands of the monomer and excimer of pyrene are centred at 400 and 500 nm, respectively. In order to study the influence of the thermal spin transition on the luminescence properties, the sample was cooled down to 10 K at 5 K min^{-1} and the luminescence spectra were recorded in the cooling and heating modes (Fig. 5a and S7†). Upon cooling to 190 K from room temperature, the intensity of both peaks, excimer and monomer, slightly increases whereas with further cooling in the region of the spin transition at around 235–155 K the intensity of the monomer signal increases significantly concomitantly with the quenching of the excimer's signal (Fig. 5a). The thermal dependence of fluorescence for the non-SCO isostructural compound **1Zn@pyr** after excitation at 332 nm shows two main maxima centred at 439 and 484 nm (Fig. 5b), whose intensity does not change significantly in the 235–155 K interval where **1Fe@pyr** displays the SCO behaviour (see Fig. 5c). Clearly the spin transition properties of **1Fe@pyr** have a strong influence on the photoluminescence properties. This observation is

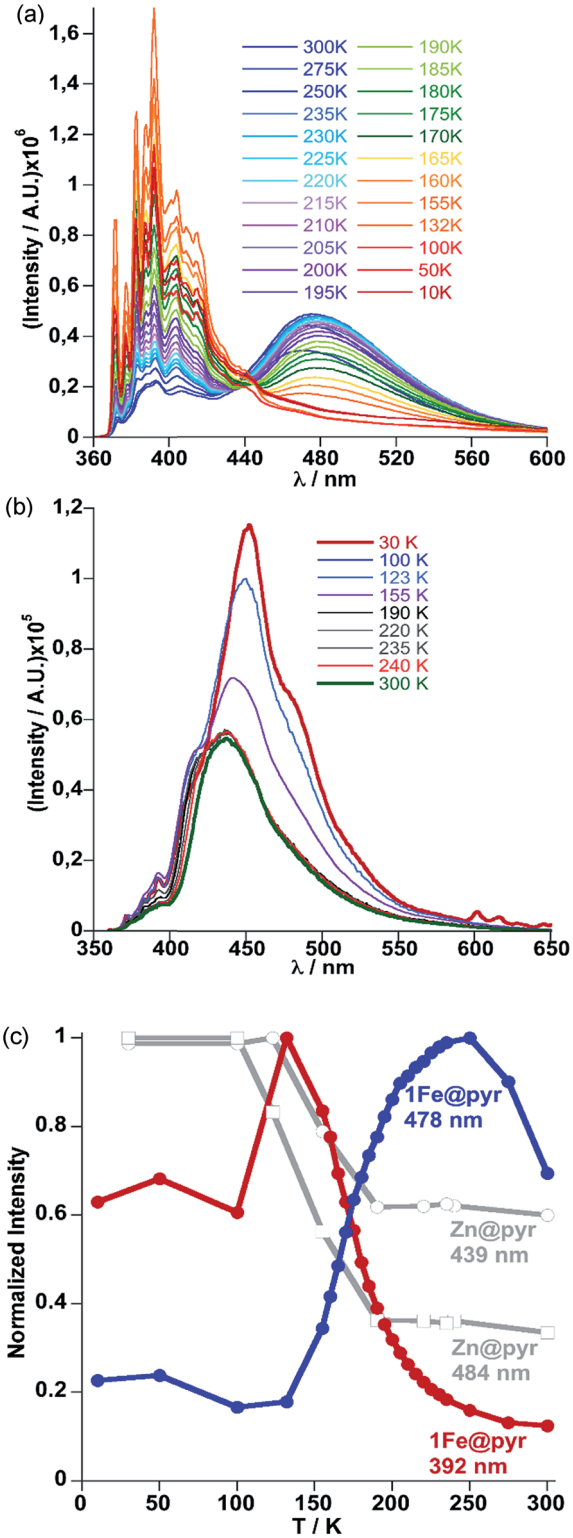

Fig. 5 (a) Evolution of fluorescence spectra with temperature upon cooling from 300 K to 10 K at 5 K min^{-1} for **1Fe@pyr**. (b) Evolution of the luminescence spectra with temperature upon cooling from 300 K to 10 K at 5 K min^{-1} for **1Zn@pyr**. (c) Thermal dependence of normalized intensity of the monomer and excimer signals at 392 nm (red) and 478 nm (blue) for **1Fe@pyr** and 439 nm and 484 nm (grey) for **1Zn@pyr**.

directly related to the absorption properties of the compound and the emission properties of the pyrene. The arising of the LS absorption band at 532 nm (Fig. 4a) upon cooling quenches the emission of the excimer signal of pyrene at 478 nm (Fig. 5a) due to the radiative energy transfer (emission–reabsorption) from the excited state of the pyrene to the MLCT-3d ($^1A_1 \rightarrow {}^1T_1$) band of the Fe^{II} complex in the LS state. The signal at 392 nm, that abruptly increases below the spin transition, overlaps with the MLCT-3d ($^1A_1 \rightarrow {}^1T_1$) transition band of the compound at any temperature. From the ratio between the intensity at 392 nm and 478 nm while heating and cooling at 5 K min^{-1} the thermal evolution of the normalized HS molar fraction $(\gamma_{HS})^{norm}$ has been obtained. The thermal spin transition stablished based on the luminescence properties of **1Fe@pyr** follows reasonably well the SCO profile obtained by absorption spectroscopy and magnetic measurements (Fig. 6). The differences observed, particularly at low temperatures, can be ascribed, on one hand, to the much more rapid temperature scan rate used for recording the SCO by luminescence and, on the other hand, to the difficulties to separate the increasing signal of the monomer emission from that of the exciplex as temperature decreases. In spite of this, the average equilibrium temperature at which $(\gamma_{HS})^{norm} = 0.5$, $T_{1/2} = 189.5$ K, centred in the middle of a hysteresis loop *ca.* 5 K wide, is virtually the same as that observed from magnetism and absorption spectroscopy. In a recent study, likely inspired by the complex $[Fe(abpt)_2(NCS)_2]$ with abpt = 4-amino-3,5-bis(pyridine-2-yl)-1,2,4-triazole,[35] pyrene was covalently coupled by condensation of 1-pyrenecarboxaldehyde with abpt to afford (pyrene-1-yl)-*N*-(3,5-di(pyridin-2-yl)-4*H*-1,2,4-triazol-4-yl)methanimine (L).[14] The resulting $[Fe(L)_2(NCS)_2]$ compound undergoes a SCO in the interval 200–350 K with $T_{1/2} = 267$ K. The pyrene moieties interact with each other defining four face-to-face π–π interactions (3.66–3.85 Å). The lack of exciplex emission well separated from the intrinsic emission of pyrene moieties precluded from delineating a neat correlation between the thermal SCO and fluorescence profiles in this compound. However, the obvious differences observed in the temperature dependence of fluorescence between $[Fe(L)_2(NCS)_2]$ and the free ligand L,

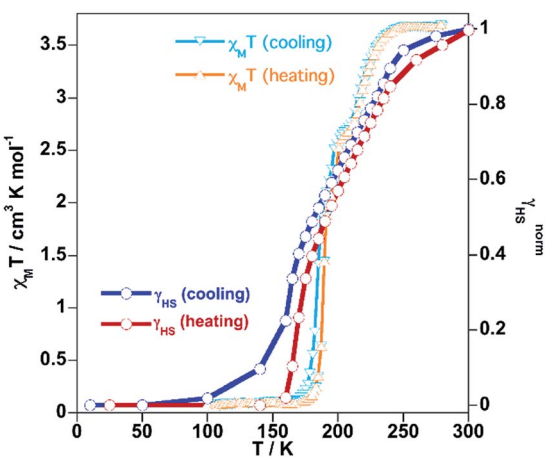

Fig. 6 Comparison of the SCO profiles obtained from magnetism and fluorescence for **1Fe@pyr**.

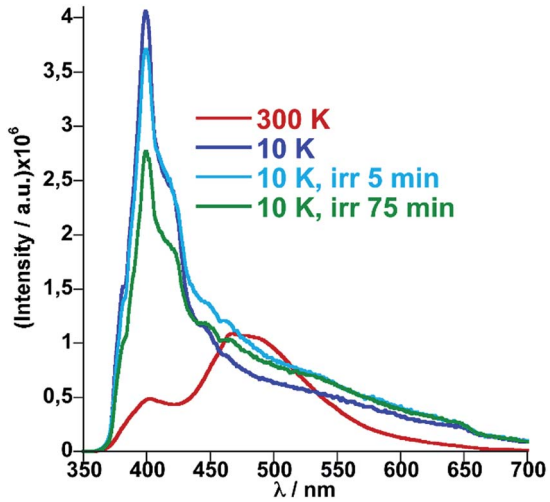

Fig. 7 Fluorescence spectra of **1Fe@pyr** at 10 K before and after irradiation at 520 nm.

associated with a resonance energy transfer process similar to that observed for **1Fe@pyr**, made possible to infer a clear influence of the SCO on the fluorescence. In particular, the partial population (*ca.* 21%) of the photo-generated HS* LIESST state of $[Fe(L)_2(NCS)_2]$ at 10 K also demonstrates this influence on the fluorescence.

Similarly, photo-excitation of the titular compound **1Fe@pyr** from LS to HS* (LIESST effect) has been preliminary followed by luminescence. In Fig. 7 the fluorescence spectra at 10 K before and after irradiation of the sample at 520 nm at two different irradiation times are compared. Interestingly, the fluorescence of the monomer decreases concomitantly with an increase of the excimer signal due to the excitation of the LS state into the metastable HS* state. In this sense, further analysis could be performed in order to study the cooperativity of the system thought LIESST and HS to LS relaxations at low temperature by taking advantage of the photoluminescence properties of pyrene.

Conclusions

In summary, we have successfully synthesized an unprecedented 3D Hofmann-type Fe^{II} SCO-CP functionalized with pyrene as a fluorescent guest. Strong π–π interactions between pyrene and the pillars of the **pcu** SCO framework result in exciplex emission. Both monomer and exciplex fluorescence are dependent on the spin state of the Fe^{II} nodes which in turn is controlled by temperature and light irradiation (LIESST effect), thereby resulting in ON–OFF switching of the luminescent signal. Implementing the prolific family of Hofmann-type SCO-MOFs with luminescence properties offers new opportunities for designing and probing devices at micro- and nano-scales for sensing and information processing. In this sense, incorporation of a luminescent source in the pillars of the framework is a further desired step. Our preliminary results in this direction are very promising and will be reported elsewhere in due course.

Conflicts of interest

There are no conflicts to declare.

Acknowledgements

This work was supported by the Spanish Ministerio de Economia y Competitividad (MINECO), FEDER (CTQ2013-46275-P and CTQ2016-78341-P), Unidad de Excelencia María de Maeztu (MDM-2015-0538), Generalitat Valenciana (PROMETEO/2016/147) and the Swiss National Science Foundation (Project number 200021-169033).

Notes and references

1 See for example:(*a*) *Spin Crossover in Transition Metal Compounds I-III. Top. Curr. Chem.*, P. Gütlich and H. A. Goodwin, 2004, vol. 233–235; (*b*) J. A. Real, A. B. Gaspar and M. C. Muñoz, *Dalton Trans.*, 2005, 2062; (*c*) A. Bousseksou, G. Molnár, L. Salmon and W. Nicolazzi, *Chem. Soc. Rev.*, 2011, **40**, 3313; (*d*) *Spin-crossover materials: properties and applications*, ed. M. A. Halcrow, John Wiley & Sons, 2013.

2 (*a*) M. Cavallini, I. Bergenti, S. Milita, J. C. Kengne, D. Gentili, G. Ruani, I. Salitros, V. Meded and M. Ruben, *Langmuir*, 2011, **27**, 4076; (*b*) P. N. Martinho, C. Rajnak and M. Ruben, in *Spin-Crossover Materials: Properties and Applications*, ed. M. A. Halcrow, Wiley, 2013, pp. 376–404; (*c*) G. Molnar, S. Rat, L. Salmon, W. Nicolazzi and A. Bousseksou, *Adv. Mater.*, 2018, **30**, 17003862.

3 H. J. Shepherd, C. M. Quintero, G. Molnar, L. Salmon and A. Bousseksou, in *Luminescent spin-crossover materials*, John Wiley & Sons Ltd., 2013, p. 347.

4 C. Piguet, E. Rivara-Minten, G. Bernardinelli, J.-C. Buenzli and G. Hopfgartner, *J. Chem. Soc., Dalton Trans.*, 1997, 421.

5 M. Matsuda, H. Isozaki and H. Tajima, *Thin Solid Films*, 2008, **517**, 1465.

6 L. Salmon, G. Molnár, D. Zitouni, C. Quintero, C. Bergaud, J.-C. Micheau and A. Bousseksou, *J. Mater. Chem.*, 2010, **20**, 5499.

7 S. Titos-Padilla, J. M. Herrera, X.-W. Chen, J. J. Delgado and E. Colacio, *Angew. Chem., Int. Ed.*, 2011, **50**, 3290.

8 C. M. Quintero, I. A. Gurals'kiy, L. Salmon, G. Molnar, C. Bergaud and A. Bousseksou, *J. Mater. Chem.*, 2012, **22**, 3745.

9 I. Suleimanov, O. Kraieva, J. Sánchez-Costa, I. O. Fritsky, G. Molnár, L. Salmon and A. Bousseksou, *J. Mater. Chem. C*, 2015, **3**, 5026.

10 I. Suleimanov, O. Kraieva, G. Molnár, L. Salmon and A. Bousseksou, *Chem. Commun.*, 2015, **51**, 15098.

11 M. Hasegawa, F. Renz, T. Hara, Y. Kikuchi, Y. Fukuda, J. Okubo, T. Hoshi and W. Linert, *Chem. Phys.*, 2002, **277**, 21.

12 H. Matzukizono, K. Kuroiwa and N. Kimikuza, *Chem. Lett.*, 2008, **37**, 446.

13 A. Santoro, L. J. Kershaw Cook, R. Kulmaczewski, S. A. Barrett, O. Cespedes and M. A. Halcrow, *Inorg. Chem.*, 2015, **54**, 682.

14 J.-L. Wang, Q. Liu, Y.-S. Meng, X. Liu, H. Zheng, Q. Shi, C.-Y. Duan and T. Liu, *Chem. Sci.*, 2018, **9**, 2892.
15 Y. Garcia, F. Robert, A. D. Naik, G. Zhou, B. Tinant, K. Robeyns, S. Michotte and L. Piraux, *J. Am. Chem. Soc.*, 2011, **133**, 15850.
16 B. Schafer, T. Bauer, I. Faus, J. A. Wolny, F. Dahms, O. Fuhr, S. Lebedkin, H.-C. Wille, K. Schlage, K. Chevalier, F. Rupp, R. Diller, V. Schünemann, M. M. Kappes and M. Ruben, *Dalton Trans.*, 2017, **46**, 2289.
17 C.-F. Wang, R.-F. Li, X.-Y. Chen, R.-J. Wei, L.-S. Zheng and J. Tao, *Angew. Chem., Int. Ed.*, 2015, **54**, 1574.
18 C. Lochenie, K. Schötz, F. Panzer, H. Kurz, B. Maier, F. Puchtler, S. Agarwal, A. Köhler and B. Weber, *J. Am. Chem. Soc.*, 2018, **140**, 700.
19 M. C. Muñoz and J. A. Real, *Coord. Chem. Rev.*, 2011, **255**, 2068.
20 Z.-P. Ni, J.-L. Liu, M. N. Hoque, W. Liu, J.-Y. Li, Y.-C. Chen and M. L. Tong, *Coord. Chem. Rev.*, 2017, **335**, 28.
21 V. Niel, J. M. Martínez-Agudo, M. C. Muñoz, A. B. Gaspar and J. A. Real, *Inorg. Chem.*, 2001, **40**, 3838.
22 A. Galet, A. B. Gaspar, M. C. Muñoz, G. V. Bukin, G. Levchenko and J. A. Real, *Adv. Mater.*, 2005, **17**, 2949.
23 (*a*) N. F. Sciortino, K. R. Scherl-Gruenwald, G. Chastanet, G. J. Halder, K. W. Chapman, J. F. Létard and C. J. Kepert, *Angew. Chem., Int. Ed.*, 2012, **51**, 10154; (*b*) M. J. Murphy, K. A. Zenere, F. Ragon, P. D. Southon, C. J. Kepert and S. M. Neville, *J. Am. Chem. Soc.*, 2017, **139**, 1330.
24 (*a*) M. Ohba, K. Yoneda, G. Agustí, M. C. Muñoz, A. B. Gaspar, J. A. Real, M. Yamasaki, H. Ando, Y. Nakao, S. Sakaki and S. Kitagawa, *Angew. Chem., Int. Ed.*, 2009, **48**, 4767; (*b*) G. Agustí, R. Ohtani, K. Yoneda, A. B. Gaspar, M. Ohba, J. F. Sánchez-Royo, M. C. Muñoz, S. Kitagawa and J. A. Real, *Angew. Chem., Int. Ed.*, 2009, **48**, 8944; (*c*) P. D. Southon, L. Liu, E. A. Fellows, D. J. Price, G. J. Halder, K. W. Chapman, B. Moubaraki, K. S. Murray, J. F. Létard and C. J. Kepert, *J. Am. Chem. Soc.*, 2009, **131**, 10998; (*d*) R. Ohtani, K. Yoneda, S. Furukawa, N. Horike, S. Kitagawa, A. B. Gaspar, M. C. Muñoz, J. A. Real and M. Ohba, *J. Am. Chem. Soc.*, 2011, **133**, 8600.
25 J. E. Clements, J. R. Price, S. M. Neville and C. J. Kepert, *Angew. Chem., Int. Ed.*, 2014, **53**, 10164.
26 V. Niel, A. L. Thompson, M. C. Muñoz, A. Galet, A. E. Goeta and J. A. Real, *Angew. Chem., Int. Ed.*, 2003, **42**, 3760.
27 (*a*) V. Meded, A. Bagrets, K. Fink, R. Chandrasekar, M. Ruben, F. Evers, A. Bernand-Mantel, J. S. Seldenthuis, A. Beukman and H. S. J. van der Zant, *Phys. Rev. B: Condens. Matter Mater. Phys.*, 2011, **83**, 245415; (*b*) F. Prins, M. Monrabal-Capilla, E. A. Osorio, E. Coronado and H. S. J. van der Zant, *Adv. Mater.*, 2011, **23**, 1545; (*c*) M. Cavallini, I. Bergenti, S. Milita, J. C. Kengne, D. Gentili, G. Ruani, I. Salitros, V. Meded and M. Ruben, *Langmuir*, 2011, **27**, 4076; (*d*) T. Miyamachi, M. Gruber, V. Davesne, M. Bowen, S. Boukari, L. Joly, F. Scheurer, G. Rogez, T. K. Yamada, P. Ohresser, E. Beaurepaire and W. Wulfhekel, *Nat. Commun.*, 2012, **3**, 938; (*e*) P. N. Martinho, C. Rajnak and M. Ruben, in *Spin-Crossover Materials: Properties and Applications*, ed. M. A. Halcrow, Wiley, 2013, p. 376 and references therein; (*f*) H. J. Shepherd, G. Molnár, W. Nicolazzi, L. Salmon and A. Bousseksou, *Eur. J. Inorg. Chem.*, 2013, 653; (*g*) A. Rotaru, J. Dugay, R. P. Tan, I. A. Guralskiy, L. Salmon, P. Demont, J. Carrey, G. Molnár, M. Respaud and A. Bousseksou, *Adv. Mater.*, 2013, **25**, 1745; (*h*) I. A. Gural'skiy, C. M. Quintero, J. Sánchez-Costa, P. Demont, G. Molnár, L. Salmon, H. J. Shepherd and A. Bousseksou, *J. Mater. Chem. C*, 2014, **2**, 2949; (*i*) A. C. Aragonés, D. Aravena, J. I. Cerdá, Z. Acís-Castillo, H. Li, J. A. Real, F. Sanz, J. Hihath, E. Ruiz and I. Díez-Pérez, *Nano Lett.*, 2016, **16**, 218.
28 (*a*) L. Piñeiro-López, M. Seredyuk, M. C. Muñoz and J. A. Real, *Chem. Commun.*, 2014, **50**, 1833; (*b*) L. Piñeiro-López, F. J. Valverde-Muñoz, M. Seredyuk, M. C. Muñoz, M. Haukka and J. A. Real, *Inorg. Chem.*, 2017, **56**, 7038.
29 J.-Y. Li, C.-T. He, Y.-C. Chen, Z.-M. Zhang, W. Liu, Z.-P. Ni and M. L. Tong, *J. Mater. Chem. C*, 2015, **3**, 7830.
30 (*a*) E. Trzop, D. Zhang, L. Piñeiro-Lopez, F. J. Valverde-Muñoz, M. C. Muñoz, L. Palatinus, L. Guerin, H. Cailleau, J. A. Real and E. Collet, *Angew. Chem., Int. Ed.*, 2016, **55**, 1; (*b*) J. E. Clements, J. R. Price, S. M. Neville and C. J. Kepert, *Angew. Chem., Int. Ed.*, 2016, **55**, 15105; (*c*) D. Zhang, E. Trzop, F. J. Valverde-Muñoz, L. Piñeiro-López, M. C. Muñoz, E. Collet and J. A. Real, *Cryst. Growth Des.*, 2017, **17**, 2736; (*d*) N. F. Sciortino, K. A. Zenere, M. E. Corrigan, G. J. Halder, G. Chastanet, J. F. Létard, C. J. Kepert and S. M. Neville, *Chem. Sci.*, 2017, **8**, 70; (*e*) M. J. Murphy, K. A. Zenere, F. Ragon, P. D. Southon, C. J. Kepert and S. M. Neville, *J. Am. Chem. Soc.*, 2017, **139**, 1330.
31 N. Ortega-Villar, M. C. Muñoz and J. A. Real, *Magnetochemistry*, 2016, **2**, 16.
32 S. Decurtins, P. Gütlich, P. C. Köhler, H. Spiering and A. Hauser, *Chem. Phys. Lett.*, 1984, **105**, 1.
33 J. F. Létard, P. Guionneau, L. Rabardel, J. A. K. Howard, A. Goeta, D. Chasseau and O. Kahn, *Inorg. Chem.*, 1998, **87**, 4432.
34 B. D. Wagner, G. J. McManus, B. Moulton and M. Zaworotko, *Chem. Commun.*, 2002, 2176.
35 (*a*) N. Moliner, A. B. Gaspar, M. C. Muñoz, S. Létard, J. F. Létard, X. Solans, R. Burriel, M. Castro, O. Kahn and J. A. Real, *Inorg. Chim. Acta*, 1999, **291**, 279; (*b*) A. B. Gaspar, M. C. Muñoz, N. Moliner, V. Ksenofontov, G. Levchenko, P. Gütlich and J. A. Real, *Monatsh. Chem.*, 2003, **134**, 285.